Elsevier Editorial System(tm) for Composites Science and Technology
Manuscript Draft

Manuscript Number: CSTE-D-13-00426R2

Title: Nanoscopic observations for evaluating the failure process of aligned multi-walled carbon nanotube / epoxy composites

Article Type: Full Length Article

Section/Category: Mechanics, modelling and analysis

Keywords: A. Carbon nanotubes, A. nano composites, B. Debonding C. Transmission electron microscopy (TEM),

Corresponding Author: Mr. tsuda terumasa,

Corresponding Author's Institution:

First Author: tsuda terumasa

Order of Authors: tsuda terumasa; tsuda terumasa; ogasawara toshio; sook-yong moon; nakamoto kengo; takeda nobuo; shimamura yoshinobu; inoue yoku

Abstract: This study examined the nanoscopic damage progression of aligned multi-walled carbon nanotubes (CNT) / epoxy composites under tensile loading using transmission electron microscopy (TEM). Aligned CNT/epoxy composite films (30 micro meter thickness) were processed using a forest-drawn aligned CNT sheet and hot-melt prepreg method. Four film specimens, respectively subjected to tensile stress of 0 MPa, 45 MPa, 95 MPa and 110 MPa, were prepared. After tensile loading, each specimen was machined until the thickness became about 100 nm using a focused ion beam milling machine (FIB) for TEM observations. Damage of three kinds, i.e. CNT break derived from the disordered CNT structures around metallic catalyst, sword-in-sheath type CNT break, and several patterns of interfacial debonding, was observed clearly. The broken CNTs and interfacial debonding per unit area were counted from TEM photographs. Results show that broken CNTs and interface debonding increased considerably at 95-110 MPa, which suggests multiple fracture of CNT under tensile loading. The CNT length at the failure stress (110 MPa) was approximately 45 μm. Estimated values from the strength of CNTs resemble those from macroscopic stress-strain behavior.

# Nanoscopic observations for evaluating the failure process of aligned multi-walled carbon nanotube / epoxy composites

Terumasa TSUDA[1*], Toshio OGASAWARA[2], Sook-young MOON[2], Kengo NAKAMOTO[3], Nobuo TAKEDA[1], Yoshinobu SHIMAMURA[4], and Yoku INOUE[4]

[1]Graduate School of Frontier Sciences, The University of Tokyo 5-1-5, Kashiwanoha, Kashiwa-shi, Chiba 277-8561, Japan

[2]Advanced Composites Technology Center, Japan Aerospace Exploration Agency (JAXA), 6-13-1, Osawa, Mitaka-shi, Tokyo, 181-0015, Japan

[3]Graduate School of Mechanical Engineering, Aoyama-Gakuin University, 5-10-1 Fuchinobe, Chuo-ku, Sagamihara-shi, Kanagawa 252-5258, Japan

[4]Faculty of Engineering, Shizuoka University, 3-5-1, Johoku, Naka-ku, Hamamatsu-shi, Shizuoka, 423-8561, Japan

**Abstract**

This study examined the nanoscopic damage progression of aligned multi-walled carbon nanotubes (CNT) / epoxy composites under tensile loading using transmission electron microscopy (TEM). Aligned CNT/epoxy composite films (30 μm thickness) were processed using a forest-drawn aligned CNT sheet and hot-melt prepreg method. Four film specimens, respectively subjected to tensile stress of 0 MPa, 45 MPa, 95 MPa and 110 MPa, were prepared. After tensile loading, each specimen was machined until the thickness became about 100 nm using a focused ion beam milling machine (FIB) for TEM observations. Damage of three kinds, i.e. CNT break derived from the disordered CNT structures around metallic catalyst, sword-in-sheath type CNT break, and several patterns of interfacial debonding, was observed clearly. The broken CNTs and interfacial debonding per unit area were counted from TEM photographs. Results show that broken CNTs and interface debonding increased considerably at 95–110 MPa, which suggests multiple fracture of CNT under tensile loading. The CNT length at the failure stress (110 MPa) was approximately 45 μm. Estimated values from the strength of CNTs resemble those from macroscopic stress–strain behavior.

Key words: **A.** Carbon nanotubes, **A.** nano composites, **C.** Transmission electron microscopy (TEM), **B.** Debonding

---

* Corresponding author
TEL. +81-04-7136-4026,  FAX +81-04-7136-4026
E-mail **tsuda@smart.k.u-tokyo.ac.jp**

## 1. Background

Since the first discovery of carbon nanotubes (CNTs) by Iijima [1], single-walled carbon nanotubes (SWNTs), and multi-walled carbon nanotubes (MWNTs) have been widely known to show high elastic modulus and high strength [2–9]. Therefore, CNTs are anticipated for use as ideal fillers for polymers to enhance their mechanical properties. Nevertheless, numerous studies for the first stage of R&D of CNT application to polymer reinforcement performed for the last two decades have failed to demonstrate their excellent mechanical, electrical, and thermal reinforcement capabilities for polymers [10–13]. The actual mechanical properties of CNT/ polymer composites are generally inferior to those of theoretical predicted properties, mainly because of poor dispersion, low volume fraction, random orientation, and weak interfacial strength between CNTs and polymers [14–16].

As described above, CNT orientation is one important factor in enhancing the mechanical properties of CNT/polymer composites. Several efforts at fabricating CNT /polymer composites with unidirectional alignment of CNTs have been conducted, such as the use of buckypaper, shear pressing from vertically aligned CNTs (VA-CNTs), and "domino-pushing" [17–23]. These results show a higher elastic modulus and strength attributable to the highly aligned nature of CNTs with high volume fraction. However, these methods are not practical because of the poor efficiency of producing aligned CNTs. For example, regarding the shear pressing method conducted by Bradford et al. [22], the specimen size is restricted because of the small substrate used to produce VA-CNTs.

For marked improvement of mechanical properties of CNT/polymer composites, an epoch-making processing method to fabricate unidirectionally aligned CNT was proposed in 2005. Horizontally aligned CNT sheets drawn from a vertically aligned CNT array were produced by Zhang et al. [24]. This method is especially anticipated for fabricating practical sizes of aligned CNTs/polymer composites because the CNT sheet size is easy to handle. Moreover, using the aligned CNT sheets, the aligned CNT / polymer composites with higher volume fraction can be fabricated easily. Several studies examining aligned CNT sheets / polymer composites have been conducted. Cheng et al. fabricated aligned CNT sheets / epoxy composites by resin transfer molding [25, 26]. The weight fraction of CNT composite was 16.5 wt%. The mechanical properties showed high tensile strength of 231 MPa, and high Young's modulus of 20.4 GPa. Furthermore, they produced 60 wt% aligned CNT / bismaleimide (BMI) composites that had 2.1 GPa strength and 169 GPa of elastic modulus that stretched randomly dispersed CNT sheet [27]. Another group has reported 3.8 GPa strength and 293 GPa of elastic modulus that stretched aligned CNT sheet, which is the highest strength and elastic modulus reported to date [28]. Several researchers have also reported other properties, such as mechanical stiffness and electrical properties of aligned CNT /polymer matrix composites [29,30].

The authors examined the mechanical properties of the aligned CNT / epoxy composites processed using hot-melt technique [31]. The prepreg method presents several advantages compared with ordinary composite molding methods such as resin infusion and resin transfer molding. A prepreg is easy to handle and enables complex structures or components production. Furthermore, aligned CNT/epoxy prepregs are applicable to press molding because CNTs are not continuous fibers. The resultant composites showed the maximum elastic modulus and ultimate tensile strength (UTS) of a 21.4 vol.% CNT /epoxy composite of 50.6 GPa and 183 MPa.

Aligned CNT/polymer composites exhibit far superior mechanical properties than conventional randomly oriented CNT composites do. Nevertheless, the mechanical properties remain inferior to those of theoretical predictions. To improve mechanical properties further, understanding the nanoscopic damage progression is indispensable. A few experiments and theoretical calculations related to CNT fracture processes have been conducted. For example, Yamamoto et al. reported the possibility of internal fracture process of MWNTs [32]. They investigated the failure mechanism of the MWNTs during crack opening at the fracture surface of

MWNT/alumina composite through single nanotube pullout tests and transmission electron microscope (TEM) observations. Their research revealed the sword-in-sheath fracture of MWNTs after pullout of MWNT and tensile testing. Based on these results, they schematically modeled the sword-in-sheath fracture of MWNTs. Our previous reports [31] also described sword-in-sheath fractures of CNTs at the fracture surface of CNT/epoxy composites after tensile testing.

Other researchers have attempted to produce theoretical models of fracture process of CNTs or CNT-reinforced composites. X. H. Huang et al. [33] simulated the fracture process of SWNTs by molecular dynamics with an applied general CA algorithm. Results showed that an initial vacancy with Stone–Wales defects occurs first at the initial vacancy sites, implying that the initial vacancy engenders the earlier advent of plastic deformation. Furthermore, critical fracture strain becomes lower than that of perfect SWCNTs, indicating that the initial vacancy causes considerable damage in CNTs. Niaki et al. [34] also simulated the fracture process of graphene sheet and SWNTs using a similar approach and reported that dynamic fracture stresses were, respectively, determined approximately 115 GPa and 122 GPa for different sizes of graphene sheet and armchair CNTs. A multiscale mechanics method used to study the deformation and fracture of CNTs embedded in a composite was presented by D. L. Shi et al. [35], who reported that the critical strain of defect nucleation of a CNT is sensitive to its chiral angle, but not to its diameter and that the constraint effect of matrix makes the CNTs easier to fracture. They also simulated the effect of some other factors such as the waviness of CNTs, the CNT–matrix interface adhesion, and the distributed residual stresses in composites. They concluded that these factors might influence the CNT fracture behaviors. However, because of the extremely small size of the CNT, direct observation of nanoscopic damage progress such as interfacial debonding, matrix cracking, and multiple fractures of CNTs in matrix under tensile loading has not been reported.

The objective of this study is to examine the nanoscopic damage progression of aligned multi-walled carbon nanotubes (MWNTs) / epoxy composites under tensile loading. Aligned CNT/epoxy composite specimens, which were processed using forest-drawn aligned CNT sheet and hot-melt prepreg method, were subjected to tensile loading. Thin samples (100 nm thick) were prepared for transmission electron microscope (TEM) observations using a focused ion beam (FIB) method. Using TEM, nanoscopic damage at each tensile stress was observed in detail.

## 2. Experiments

### 2.1 Processing of aligned CNT sheets

Inoue et al. established a simple and efficient synthesis method for producing vertically aligned long MWCNTs using iron chloride powders as precursor of a catalyst [36]. The MWCNTs with length exceeding 1 mm were grown on a bare $SiO_2$ substrate using conventional thermal chemical vapor deposition (CVD) with single gas flow (acetylene) for 20 min. In addition to such a high growth rate, well-aligned MWCNT sheets are produced easily from the MWCNT forest by pulling it out [31]. The CNT sheets have a high volume fraction without a great amount of entanglement, which are ideal properties for use in reinforcement of the composites. Respectively, their diameters and lengths are 40–70 nm and about 1 mm.

### 2.2 Processing of CNT/epoxy composites

The procedure used to produce CNT/epoxy prepreg is presented in Fig. 1(a). The B-stage un-cured epoxy resin with release paper was obtained from a commercial prepreg company. The epoxy resin consists of bisphenol-A type epoxy, novolac type epoxy, and an aromatic diamine curing agent. The areal weight of epoxy resin film is controlled as 30 g/m$^2$, with thickness of approximately 25 μm. A stacked CNT sheet was put on a PTFE sheet. Then it was covered with epoxy resin film with a release paper. Epoxy resin was impregnated into the CNT sheet at 90°C for 3 min between steel plates of a hot press. After peeling off a prepreg sheet from the release paper,

the prepreg sheet was cured at 130°C for 1.5 h between steel plates in an oven, yielding a film specimen. A steel plate was put on a stacked prepreg sheet during curing. The pressure was approximately 2.0 MPa. Details of procedures used for CNT sheet and composite fabrication have been reported elsewhere [31, 37].

The composites' microstructure was observed using a scanning electron microscope (FE–SEM, S-4700; Hitachi Ltd., Japan). The CNT weight fraction was ascertained using a thermogravimetric analyzer (TGA, TGA-6300; SII, Japan). Method of determining volume fraction of CNTs is reported elsewhere [31]. An SEM image of CNT/epoxy composite was depicted in Fig. 1(b). The CNT volume fraction, as evaluated using TGA is about 8%. The composite thickness was about 30 μm.

### 2.3 Tensile loading, sample preparation, and TEM observations

To prepare the fracture process observation specimen, tensile tests were conducted on a screw-driven mechanical testing machine (Model 5966R; Instron Corp., USA) under a constant displacement rate of 0.2 mm/min at room temperature. Geometry and dimensions of tensile test specimen are presented in Fig. 2. The longitudinal strain was measured using a non-contacting video extensometer (AVE; Instron Corp., USA). Specimens were subjected to 0 N (0 MPa), 4 N (45 MPa), 8.5 N (95 MPa), and 10 N (110 MPa, fracture load). The thickness was measured carefully using a digital micrometer.

After tensile loading, each sample was cut carefully into a rectangular piece (5 mm long, 1.5 mm wide) and set on a TEM tip-on holder (EM-02210; JEOL). Thin samples for TEM observations were prepared using a focus ion beam milling machine (FIB, JEM-9320; JEOL). A schematic drawing and FIB image are presented respectively in Figs. 3(a) and 3(b). The machined area is approximately 30 μm wide, 4 μm deep, and 0.1 μm thick. In Fig. 3(b), CNTs are aligned from left to right. Nanoscopic observations of CNTs and CNT/epoxy interfaces were conducted using an FE-TEM (JEM-2100F; JEOL, Japan) under the accelerated electron voltage of 200 kV.

## 3. Results and Discussion

### 3.1 Stress–strain behavior of CNT/epoxy composites

Typical stress–strain curves of epoxy and CNT (8.1 vol.%) /epoxy composite are presented in Fig. 4. The Young's modulus and ultimate tensile strength (UTS) of a CNT/epoxy composite were 20.3 GPa and 111 MPa. These values were, respectively, 8.1 and 1.8 times those of the epoxy resin. The resultant composite exhibits higher Young's modulus and tensile strength than those of neat resin.

### 3.2 Classification of nanoscopic damage after tensile loading

TEM photographs portraying nanoscopic damage are presented in Figs. 5(a)–5(f). Before tensile loading (0 MPa), no CNT break or interfacial debonding was observed, as presented in Fig. 5(a). Epoxy is well impregnated into the composite. Most CNTs are well aligned.

After tensile loading (>40 MPa), damage of three kinds is clearly observed: internal fracture from disordered CNT structures around metallic catalyst, sword-in-sheath fracture, and interfacial debonding of several kinds. Figure 5(b) shows a typical CNT break feature from disordered CNT structures around an Fe inclusion. Fe was used as catalyst for CNT growth process, which is derived from the pyrolysis of $FeCl_2$ . Such a part is regarded as an easily broken point because the CNT wall growth is disturbed by the metallic catalyst. It can be speculated that local strength becomes weak at this point. Figure 5(c) depicts sword-in-sheath fracture of CNTs in the composites. This fracture mode was observed in specimens subjected to stress of less than 110 MPa (failure stress). Sword-in-sheath fractures have been observed at the fracture surface of

CNT/epoxy composites, CNT / alumina composites [31, 32] and at fracture surfaces after MWNT pull-out testing [4]. The sword-in-sheath fractures were first observed inside composites below failure stress. This result is an important experimental finding that is expected to be useful to discuss the failure mechanism of CNT/epoxy composites. This experimentally obtained result suggests that multiple fractures of CNT occur in CNT/epoxy composites.

CNT/epoxy debonding is mainly observed around disordered CNT structures, such as "bamboo like" structures (Fig. 5(d)), and bent structures (Fig. 5(e)) at 45 and 95 MPa. An Fe nanoparticle included in CNT is clearly observed in both, which suggests that Fe catalyst often acts as an origin of disordered CNT growth. Bamboo-like and bent CNT structures cause stress concentration, resulting in debonding at low stress. Furthermore, some interfacial debonding along ordered CNT is also observed at the failure stress (110 MPa), as presented in Fig. 5(f).

### 3.3 Semi-quantitative evaluation of damage progression

About 10 of TEM photographs, which correspond approximately to 120–170 $\mu m^2$ of observation area, were taken for each specimen subjected to each tensile stress. The CNTs, broken portions of CNTs, and interfacial debonding regions were counted carefully. The results are presented in Table 1. The CNT break and CNT/matrix debonding increase numerically concomitantly with increasing tensile stress.

The CNT breaks per unit area (counts /$\mu m^2$) are presented as a function of tensile stress in Fig. 6. They increase from 0.007 /$\mu m^2$ to 0.05 /$\mu m^2$ at the first loading step (0– 45 MPa). In this stage, CNT-breaks of which the origin is disordered CNT structures around metallic catalyst mainly occurred as presented in Fig. 5(b). Although the number of CNT breaks changes only slightly between the first and the second steps (45–95 MPa), CNT-breaks increased considerably at the final step (95–110 MPa) from 0.05 /$\mu m^2$ to 0.14 /$\mu m^2$. At the final stage, many sword-in-sheath CNT breaks in the matrix resin were observed, as presented in Fig. 5(c).

Fig. 7 presents the number of interfacial debonding instances per unit area (counts /$\mu m^2$). The debonding gradually increased numerically along with increasing tensile stress: 0005 /$\mu m^2$ at 0 MPa, 0.02 /$\mu m^2$ at 45 MPa, 0.13 /$\mu m^2$ at 95 MPa, and 0.38 /$\mu m^2$ at 110 MPa. As described above, debonding under the stress of 45 and 95 MPa is mainly observed around disordered CNT structures such as "bamboo like" structure, and bent structures as presented in Figs. 5(d) and 5(e). However, interfacial debonding along ordered CNT increased at the final loading step (95 MPa -> 110 MPa), as presented in Fig. 5(f).

The damage process associated with increasing tensile stress can be summarized as follows:

1. At the first loading step (0–45 MPa), the internal fracture of CNT at disordered CNT structures around metallic catalyst depicted in Fig. 5(b) is mainly observed.
2. At the second loading step (45–95 MPa), interfacial debonding disordered the "bamboo like" structure and bent structure, as presented in Figs. 5(d) and 5(e) are mainly observed, although the fracture of CNTs proceeded only slightly.
3. At the final loading step (95–110 MPa), sword-in-sheath fracture of CNT as presented in Fig. 5(c), and interfacial debonding along the ordered CNT, as presented in Fig. 5(f), are observed.

### 3.4 Estimation of multiple fracture of CNT under tensile loading

TEM observations imply that multiple fractures of CNT occur under tensile loading. The average length of broken CNTs, $l_f$, was estimated using the following equation.

$$l_f = \frac{1}{k}\sum_{i=1}^{n} l_i \quad (1)$$

Therein, $n$ denotes the number of CNTs, $l_i$ represents the length of each CNT, and $k$ stands for the number of broken CNTs throughout the observation area. The relation between stress and the average length of broken CNT, $l_f$ is presented in Fig. 8 and Table 2. Before tensile loading (0 MPa), the average CNT length was about 1100 μm, which is almost equal to the original length of CNT.

The average CNT length decreased to 120–150 μm during the first and the second loading steps (0–45 MPa, 45–95 MPa) because of the internal fracture disordered CNT structures around the metallic catalyst. During the final loading step (95–110 MPa), the CNT length decreases significantly because of sword-in-sheath fracture, and caused about 45 μm. The Fe inclusions and disordered CNT structures affect the CNT strength considerably, but these defects might not affect the composite strength because the critical CNT length is much shorter than the defect intervals in a CNT.

The relation between characteristic tensile strength of the CNT $\sigma_{CNT}$ and critical CNT (fiber) length ($L_{cr}$) is written as the following equation under the Kelly-Tyson assumption.

$$L_{cr}/2 = \sigma_{CNT} R/2\,\tau_{interface} \quad (2)$$

In that equation, $R$ denotes the CNT radius; $\tau_{interface}$ signifies the interfacial strength (IFSS) between the CNT and polymer. The CNT radius measured from TEM photographs is approximately 26.1 nm. The critical CNT (fiber) length ($L_{cr}$) is about 45 μm. The authors established the measurement method to determine the IFSS of CNT /PEEK composites [38] and applied it to a VGCF/ Bisphenol-F-type epoxy composite. The IFSS ($\tau_{interface}$) was estimated as 20 MPa [39]. The characteristic tensile strength of the CNT was calculated as 34.2 GPa. The resultant characteristic tensile strength of the CNT approaches the theoretical strength of CNTs described in previous reports, as shown in Table 3 [5–8].

### 3.5 **Discussion**

#### 3.5.1 Stress transfer of CNT

As presented in Fig. 5(c), many sword-in-sheath fractures exist during the tensile process. The average fracture interval length was 44.6 μm after fracture, which suggests the possibility that the stress transfer between layers of CNT is insufficient.

The load transfer at the interlayer in a MWCNT is roughly calculated. When the outermost layer of MWCNT fractures at the tensile load $F_{all}$, as shown in Fig. 9, the load balance between

tensile load and interfacial shear load at the CNT/matrix interface are written as shown below.

$$F_{all} = 2\pi R \tau_{interface}(L_{cr}/2) \quad (3)$$

Therein, the $\tau_{interface}$ represents the interfacial shear strength ($\tau_{interface}$) between the CNT and polymer. The load applied to the inner layer of CNT ($F_{inner}$) is written as the following equation using interfacial strength between layers of CNT ($\tau_{interwall}$):

$$F_{inner} = 2\pi(R - 2\Delta R) \tau_{interwall}(L_{cr}/2). \quad (4)$$

In that equation, $R$ is the CNT diameter, $\Delta R$ is the distance between each layer of CNTs (0.34 nm [38]) and $L_{cr}$ is the average fracture interval (44.6 μm). The value of $\tau_{interwall}$ was stated in earlier reports of the literature [40–42]. Finally, $\tau_{interface}$ is assumed to 20 MPa, as described previously [39].

The results show that $F_{all}$ from eq. (3) is 73.0 μN, $F_{inner}$ from eq. (4) is 0.3–2.3 μN and the load transfer efficiency between layers $\eta$ (= $F_{inner}/F_{all}$) is 0.4–3.3%, which means that load transfer at the interlayer in MWCNT is extremely weak, and that interfacial debonding or slippage between layers of CNT readily occurs as does sword-in-sheath fracturing.

3.5.2 Estimation of CNT strength

When the critical CNT length and IFSS are 44.6 μm and 20 MPa respectively, then the CNT strength is calculated theoretically as 34.2 GPa using equation (2). The average fracture length (44.6 μm) estimated from TEM observations should be regarded as the maximum critical CNT length because it is impossible to observe all CNT fractures using TEM.

More realistic CNT length can be estimated from the pull-out length after tensile testing. Figure 10 presents an SEM micrograph showing a pulled-out CNT from a specimen after tensile testing. Pulled-out CNTs are exposed. The pulled-out CNT length is 1.0–7.4 μm; the average length is 4.1 μm. The critical fiber length $L_{cr}$ is obtained simply from the exposed CNT length, $L_{exposed}$ as follows [43].

$$L_{cr} = L_{exposed}/4 \quad (5)$$

The critical CNT length is estimated as 4.0–29.5 μm (16.6 μm average), which is almost reasonable compared with the direct TEM observation result (44.6 μm). When the IFSS between CNT and matrix is 20 MPa, the critical strength of CNTs is 3.2–22.7 GPa (12.7 GPa average).

The elastic modulus of CNTs is much higher than that of epoxy. It is therefore reasonable to assume that the tensile load is subjected mainly to CNTs. At the failure stress of the CNT/epoxy composite (110 MPa), each CNT is subjected to approximately 1.36 GPa because the CNT volume fraction is 0.081. This value is much lower than the CNT strength described above. The effect of fiber strength distribution should be considered. Curtin [43] proposed a tensile strength prediction model based on a Weibull distribution. The tensile strength of composites with multiply-fractured

fibers can be written as

$$\sigma = V_f \sigma_f \left( \frac{2}{m+2} \right)^{\frac{1}{m+1}} \left( \frac{m+1}{m+2} \right) \quad (6)$$

where $m$ stands for the Weibull parameter. Unfortunately, the Weibull parameter for the strength of CNTs has not been reported. Assuming this value as $m$ = 5, then tensile strength is estimated as 1.94 GPa. This result still shows a difference from the estimation from average fracture length and pullout length of CNTs. One possible reason is that the interfacial shear strength used in this estimation (20 MPa) is too high. The authors have evaluated the interfacial shear strength (IFSS) of CNT/PEEK and CNT/epoxy composites using a nano-pullout method [38]. Results show that the IFSS of specimens after tensile testing decreased as compared with pristine specimens. That is true because of partial debonding at the interface between CNT and matrix before final failure. Actually, the partial interfacial debondings are observed clearly during the tensile process, as presented in Fig. 5(f). Therefore the IFSS used for the strength estimation (= 20 MPa) should be regarded as a maximum value.

The IFSS of CNT/epoxy composites becomes lower under the existence of the interfacial debondings. Our earlier report described that IFSS of VGCF/bisphenol-F-type epoxy composites after tensile testing was measured as about 5 MPa [39]. Under the assumption of interfacial debonding, estimations of tensile strength by TEM photographs and SEM micrographs becomes smaller: 8.9 GPa and 3.3 GPa. These results are close to the result of eq. (6), indicating that our experiments were conducted with some validity.

However, when only outermost wall (diameter of 52 nm and interlayer is assumed to be 0.34 nm) are taken into account, strength estimation causes some mismatch. From the microscopic observation by TEM, the strength of MWNT becomes 1307 GPa when interfacial damage was ignored, 342 GPa when interfacial damage was taken into account. These values was extremely high compared with previous reports [5-8]. One reason of the strength overestimating is limitation of the observation area. As shown in Fig.2, tensile test specimen is 30 mm in length, 3 mm in width. But microscopic observation area is only 30 μm in length, 4 μm in depth due to the milling limitation of FIB. Then it is thought that quantitative evaluation from the microscopic observation by TEM includes locality and precise evaluation became difficult.

Same approach was conducted for strength calculation to the exposed CNTs at the fracture surface. Then the strength of MWNT became 488 GPa when interfacial damage was ignored, 127 GPa when interfacial damage was taken into account. These values are in the same order of previous reports [5-8], but still high. If same approach was applied to the stress estimation which was obtained from stress-strain curve, the results is obtained to 52.3 GPa and 74.7 GPa, which values are near the previous reports [5-8].

Another possibility of strength overestimating is load distribution to the inner walls. CNTs used in this study are about 1 mm in length, which value is much longer than previous reports (aspect ratio >20,000). Even during tensile testing length of CNT is still much bigger than previous CNTs, as shown in Fig.8 (aspect ratio>2,000 before final fracture). Therefore it is thought that load distribution of inner walls should be taken into account even if interfacial strength between CNT walls is weak. Then the load which applied to outermost wall is reduced and then strength is also reduced.

Other factors for differentiating the strength of CNTs are alignment of CNTs, invisible fractures, matrix cracking and so on. TEM observation method includes some problems. For the TEM observation, specimen size and observation area are considerably limited in comparison with true size of CNT due to the limitation of the FIB milling ability and observation magnification. There are many CNTs that orientation was not aligned to the tensile direction or bended to the other direction, as shown in Fig.5(c), (e). These CNTs are not straight such as CNTs exposed at the

fracture surface, which causes the error in the strength calculation.

And TEM observation includes the missing point which could not be observed. For example, defects which cannot be distinguished from an internal break of CNT, very thin diameter of CNT, agglomerated CNT and so on. Considering these factors, results for estimating the strength of CNT is correct to some degrees.

## 4. Conclusions

To observe the microscopic damage of the composites during the tensile process, the FIB milling method technique for observing internal fracture by TEM was applied. Multiple fractures of CNT and interfacial debonding between CNT and polymer during the tensile process were observed. The maximum interval fracture length was 44.6 μm after tensile testing.

Sword-in-sheath fractures of CNTs were observed, indicating that the load transfer at the interlayer in a MWCNT is weak. The theoretical strength of CNT was estimated from the stress–strain curve including the Weibull parameter of CNT and 1.94 GPa, which value is close to the estimations from microscopic observation by TEM and exposed length of CNTs at the fracture surface by SEM, assuming orientation of CNTs, interfacial debonding between the CNT and polymer, matrix cracking, load transfer between walls of CNT and so on. Considering these error factors the result is in the proper range. How to treat these factors is the future work.

## 5. Acknowledgments

This study was supported by the Japan Society for the Promotion of Science (JSPS: subject number 24・5047) and the Japan Science and Technology Agency Advanced Low Carbon technical development program (ALCA).

## References

1. Iijima S. Helical microtubes of graphic carbon. Nature 1991;354:56–58.
2. Krishman A, Dujardin E, Ebbesen TW, Yianilos PN, Treacy MMJ. Young's modulus of single-walled carbon nanotubes. J Appl Phys 1998;84:1939–1943.
3. Sinnott SB, Andrews R. Carbon Nanotubes: Synthesis, Properties, and Applications. Critical Reviews in Solid State and Materials Sciences 2001;26 (3):145–249.
4. Salvetat JP, Kulik AJ, Bonard JM, Forro L, Benoit W, Auppironi L. Mechanical properties of carbon nanotubes. Appl Phys A 1999;69:255–260.
5. Yu MF, Lourie O, Dyer MJ, Moloni K, Kelly TF, Ruoff RS. Strength and breaking mechanism of multiwalled carbon nanotubes under tensile load. Science 2000;287(5453):637–640.
6. Demcayk BG, Wang YM, Cumings J, Hetman M, Han W, Zettl A, Ritchie RO. Direct mechanical measurement of the tensile strength and elastic modulus of multiwalled carbon nanotubes. Mater Sci Eng A 2002;334:173–178.
7. Pan ZW, Xie SS, Lu L, Chang BH, Sun LF. Tensile tests of ropes of very long aligned multiwall carbon nanotubes. Appl Phys Lett 1999;74:3152–3154.
8. Peng B, Locascio M, Zapol P, Li SY, Mielke SL, Schatz GC. Espinosa HD. Measurements of near-ultimate strength for multiwalled carbon nanotubes and irradiation-induced crosslinking improvements. Nat Nanotechnol 2008;3:626–631.
9. Ruoff RS, Qian D, Liu W. Mechanical properties of carbon nanotubes:theoretical predictions and experimental measurements. C R Physique 2003;4:993–1008.
10. Thostenson ET, Ren Z, Chou T-W. Advances in the science and technology of carbon

nanotubes and their composites: a review. Compos Sci Technol 2001;61:1899–1912.
11. Coleman JN, Khan U, Blau WJ, Gun'ko YK. Small but strong: A review of the mechanical properties of carbon nanotube–polymer composites. Carbon 2006;44:1624–1652.
12. Gojny FH, Wichmann MHG, Kopke U, Fiedler B, Schulte K. Carbon nanotube-reinforced epoxy-composites: enhanced stiffness and fracture toughness at low nanotube content. Composite Science and Technology 2004;64(15):2361–2371.
13. Guo P, Chen X, Gao X, Song H, Shen H. Fabrication and mechanical properties of well-dispersed multiwalled carbon nanotubes / epoxy composites. Composite Science and Technology 2007;67(15–16):3331–3337.
14. Thostenson ET, Chou T-W. On the elastic properties of carbon nanotube-based composites: modeling and characterization. J Phys D: Appl Phys 2003;36:573–582.
15. Schadler LS, Giannaris SC, Ajayan PM. Load transfer in carbon nanotube epoxy composites. Appl Phys Lett 1998;73:3842–3844.
16. Ogasawara T, Tsuda T, Takeda N. Stress–strain behavior of multi-walled carbon nanotube / PEEK composites. Composite Science and Technology 2011;71(2):73–78.
17. Wang Z, Liang Z, Wang B, Zhang C, Kramer L. Processing and property investigation of single-walled carbon nanotube (SWNT) buckypaper / epoxy resin matrix nanocomposites. Composites Part A 2004;35:1225–1232.
18. Lopes PE, Hattum F, Pereira CMC, Nóvoa PJRO, Forero S, Hepp F, Pambaguian L. High CNT content composites with CNT buckypaper and epoxy resin matrix: Impregnation behavior composite production and characterization. Composite Structures 2010;92:1291–1298.
19. Wardle BL, Saito DS, Garcia EJ, Hart AJ, Villoria RGD, Verploegen EA. Fabrication and characterization of ultrahigh-volume-fraction aligned carbon nanotube–polymer composites. Adv Mater 2008;20(14):2707–2714.
20. Cebeci H, Villoria RG, Hart AJ, Wardle BL. Multifunctional properties of high volume fraction aligned carbon nanotube polymer composites with controlled morphology. Composites Science and Technology 2009;69:2649–2656.
21. Chou T-W, Gao L, Thostenson ET, Zhang Z, Byun J-H. An assessment of the science and technology of carbon nanotube-based fibers and composites. Composites Science and Technology 2010;70 (1):1–19.
22. Bradford PD, Wang X, Zhao H, Maria J-P, Jia Q, Zhu YT. A novel approach to fabricate high volume fraction nanocomposites with long aligned carbon nanotubes. Composites Science and Technology 2010;70(13):1980–1985.
23. Wang D, Song PC, Liu CH, Wu W, Fan SS. Highly oriented carbon nanotube papers made of aligned carbon nanotubes. Nanotechnology 2008;19(7):075609.
24. Zhang M, Fang S, Zakhidov AA, Lee SB, Aliev AE, Williams CD, Atkinson KR, Baughman RH. Strong, transparent, multifunctional, carbon nanotube sheets. Science 2005;309(5738):1215–1219.
25. Cheng Q-F, Wang J-P, Wen J-J, Liu C-H, Jiang K-L, Li Q-Q, Fan S-S. Carbon nanotube/epoxy composites fabricated by resin transfer molding. Carbon 2010;48:260–266.
26. Cheng Q-F, Wang JP, Jiang K-L, Li Q-Q, Fan S-S. Fabrication and properties of aligned multiwalled carbon nanotube-reinforced epoxy composites. J Mater Res 2008;23 (11):2975–2983.
27. Cheng Q-F, Bao J, Park J, Liang Z, Zhang C, Wang B. High Mechanical Performance Composite Conductor:Multi-Walled Carbon Nanotube Sheet/ Bismaleimide Nanocomposites. Advanced Functional Materials 2009;19 (20):3219–3225.
28. X. Wang, Z. Z. Yong, Q. W. Li, P. D. Bradford, W. Liu, D. S. Tucker, W. Cai, H. Wang, F. G. Yuan, Y. T. Zhu. Ultrastrong, Stiff and Multifunctional Carbon Nanotube Composites. Mater Res Lett 2013;1:19-25.

29. Shim BS, Zhu J, Jan E, Critchley K, Ho S, Podsiadlo P, Sun K, Kotov NA. Multiparameter structural optimization of single-walled carbon nanotube composites: toward record strength, stiffness, and toughness. ACS Nano 2009;3(7):1711–1722.
30. Mora RJ, Vilatela JJ, Windle AH. Properties of composites of carbon nanotube fibers. Composites Science and Technology 2009;69:1558–1563.
31. Ogasawara T, Moon SY, Shimamura Y, Inoue Y. Mechanical properties of aligned multi-walled carbon nanotube / epoxy composites processed using a hot-melt prepreg method. Comp Sci Technol 2011;71:1826–1833.
32. Yamamoto G, Shirasu K, Hashida T, Takagi T, Suk JW, An J, Piner RD, Ruoff RS. Nanotube fracture during the failure of carbon nanotube / alumina composites. Carbon 2011;49:3709–3716.
33. Huang XH, He XQ. Fracture analysis of carbon nanotubes in the context of an atomic-based cellular automata algorithm. Comp Mat Sci 2012;65:85–90.
34. Niaki SA, Mianroodi JR, Sadeghi M, Naghdabadi R. Dynamic and static fracture analysis of grapheme sheets and carbon nanotubes. Comp Struc 2012:94;2365–2372.
35. Shi D-L, Feng X-Q, Jiang H, Huang YY, Hwang K-C. Multiscale analysis of fracture of carbon nanotubes embedded in composites. Inter J of Frac 2005;134:369–386.
36. Inoue Y, Kakihata K, Hirono Y, Horie T, Ishida A, Mimura H. One-step grown aligned bulk carbon nanotubes by chloride mediated chemical vapor deposition. Appl Phys Lett 2008;92(21):213113.
37. Inoue Y, Suzuki Y, Minami, Y, Muramatsu J, Shimamura Y, Suzuki K, Ghemes A, Okada M, Sakakibara S, Mimura H, Naito K. Anisotropic carbon nanotube papers fabricated from multiwalled carbon nanotube webs. Carbon 2011;49 (7):2437–2443.
38. Tsuda T, Ogasawara T, Deng F, Takeda N. Direct measurements of interfacial shear strength of multi-walled carbon nanotube/PEEK composite using a nano-pullout method. Comp Sci Technol 2011;71:1295–1300.
39. Tsuda T, Ogasawara T, Takeda N. Interfacial shear strength of MWNT /epoxy composites and comparison with molecular dynamics simulation. Proc. of 18th International Conference on Composites Materials (ICCM), Jeju, Korea (2011) F25-5-AF1210.
40. Cui S, Kinloch IA, Young RJ, Noe´ L, Monthioux M. The Effect of Stress Transfer Within Double-Walled Carbon Nanotubes upon their Ability to Reinforce Composites. Adv Mater 2009;21:3591–3595.
41. Zalamea L, Kim H, Pipes RB. Stress transfer in multi-walled carbon nanotubes. Comp Sci Technol 2007;67:3425–3433.
42. Viet NV, Kuo WS. Load transfer in fractured carbon nanotubes under tension, Comp B 2012;43:332–339.
43. Curtin WA. Theory of Mechanical Properties of Ceramic-Matrix Composites. Journal of the American Ceramic Society 1991;74:2837–2845.

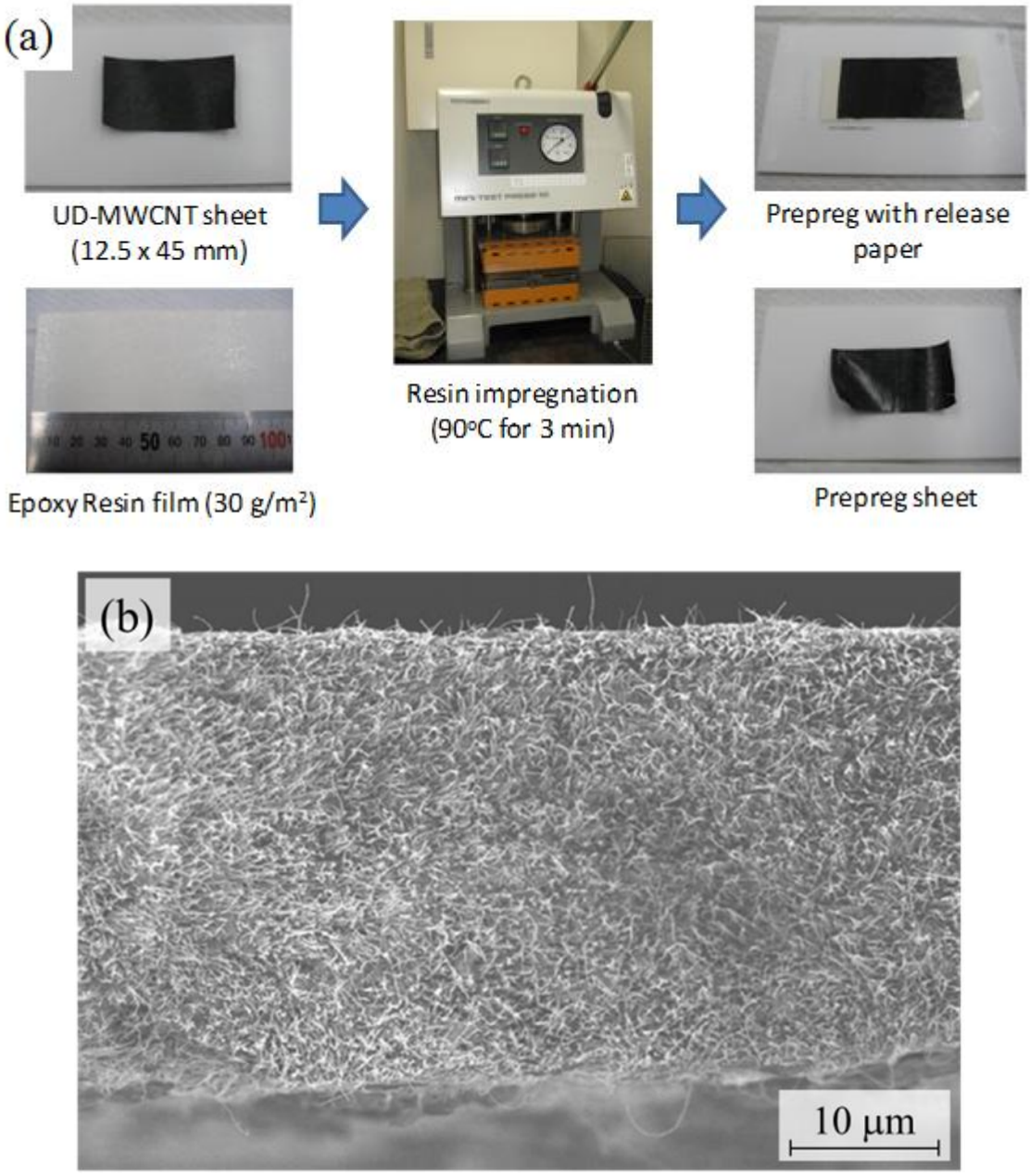


Fig. 1(a) Photographs showing processing of an aligned CNT/ epoxy prepreg using the hot-melt method [29] and (b) SEM image of Aligned CNT/epoxy composite film.

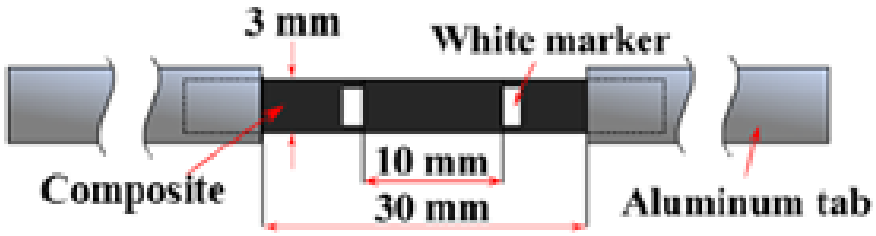


Fig. 2 Specimen for tensile testing.

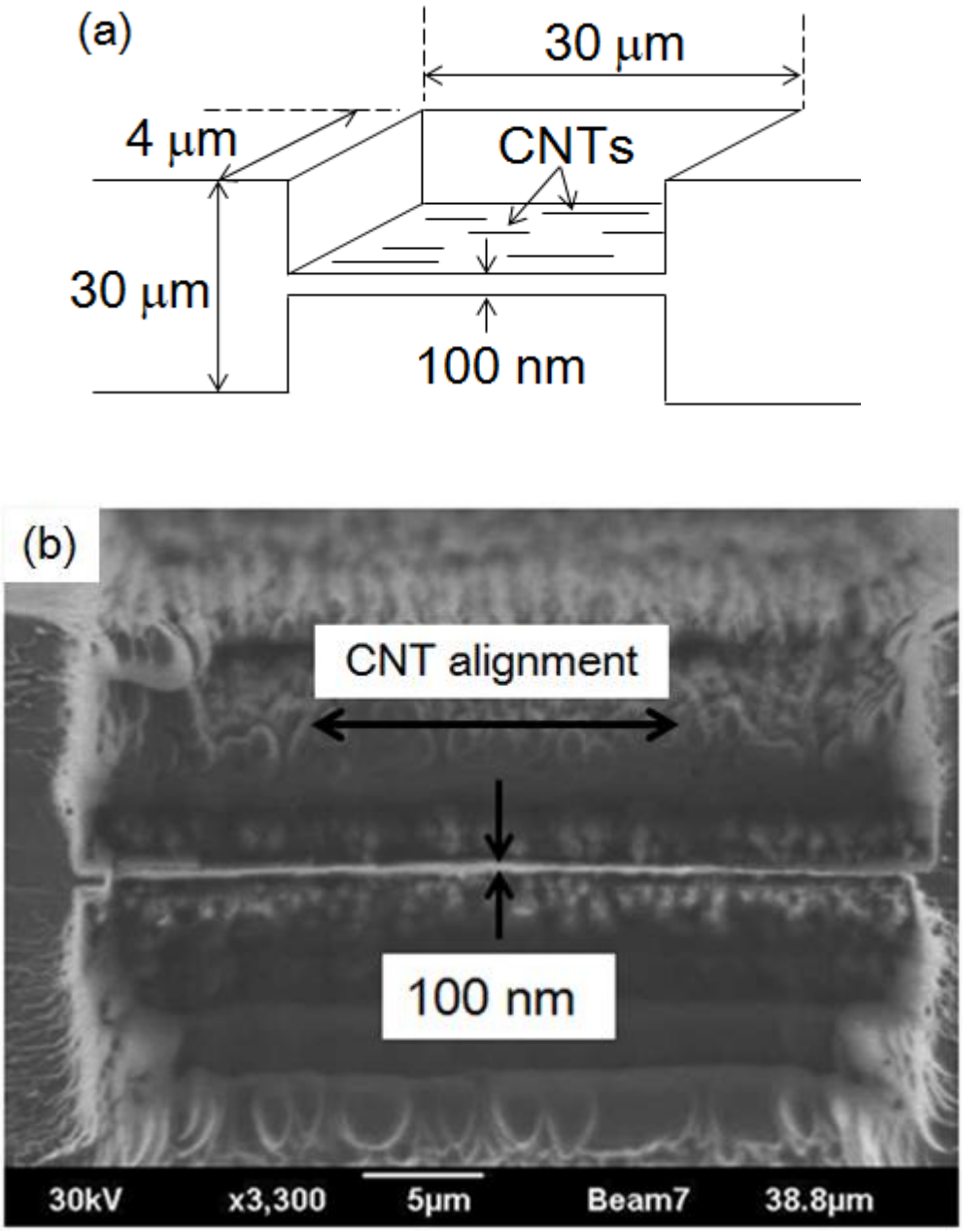


Fig. 3 Sample for internal observation (a) illustration of milled sample and (b) actual FIB image of milled sample.

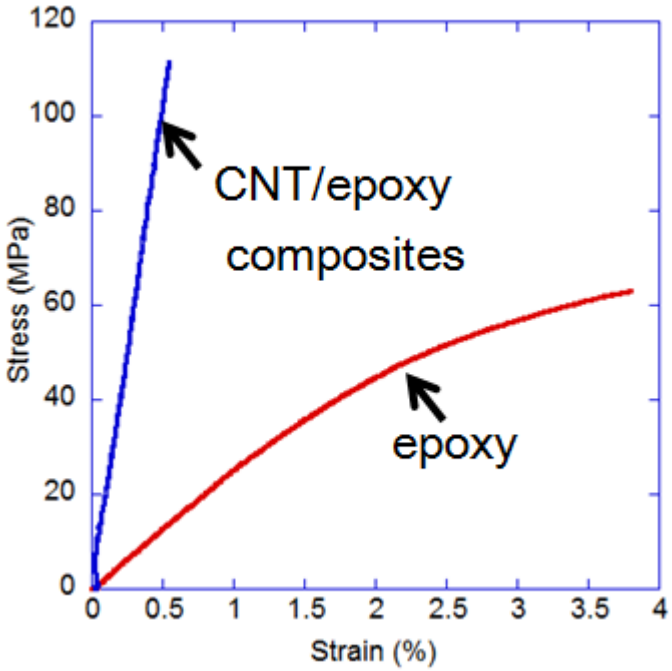

Fig. 4 Typical stress–strain curve of the composites. Volume fraction of CNT is 8.1%.

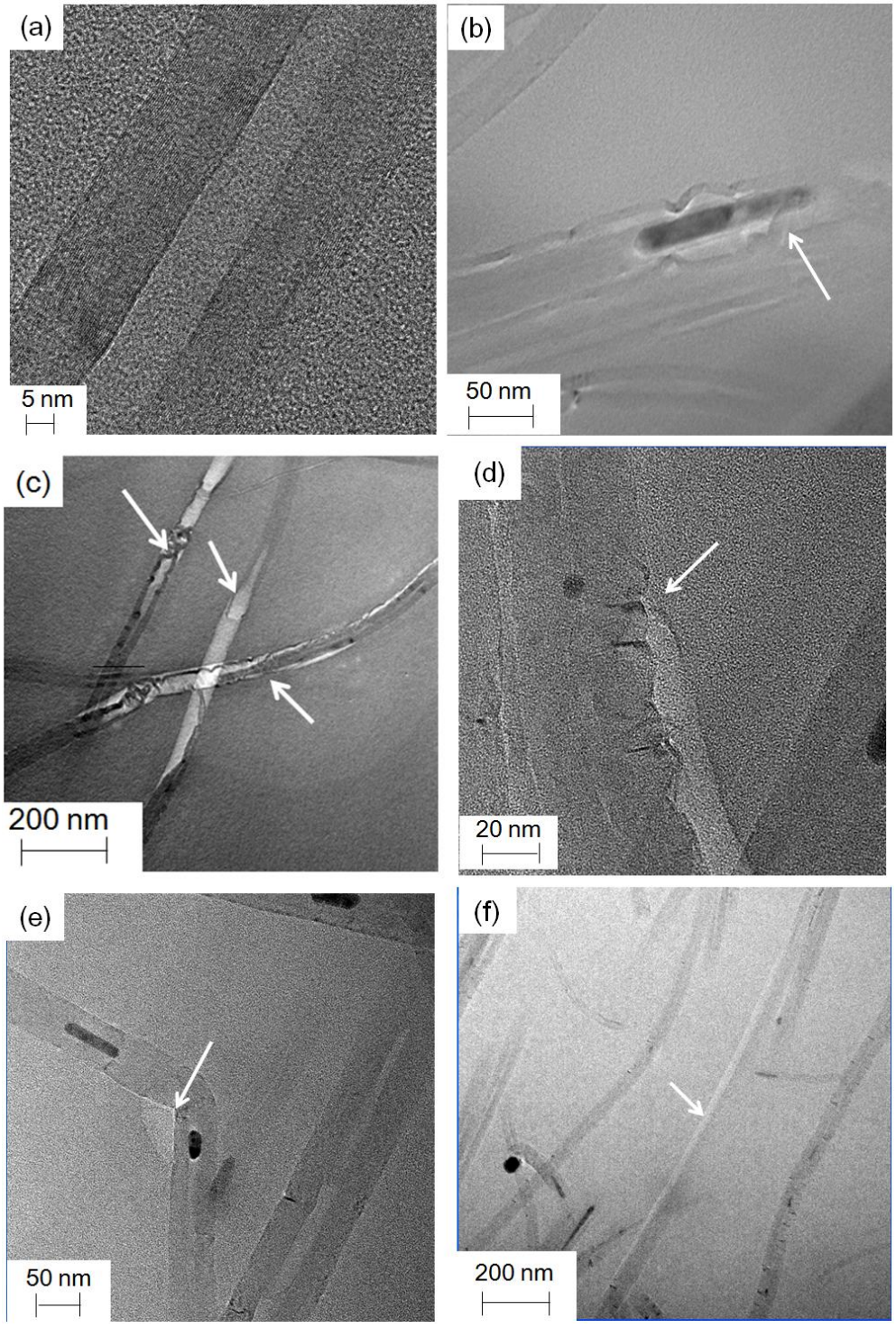


Fig. 5 Microscopic observation results. (a) CNT inside the composites (at 0 MPa), (b) internal fracture at the metallic catalyst (at 45 MPa), (c) sword-in-sheath fracture of CNT (at 110 MPa), (d) interfacial debonding at "Bamboo" structure (at 95 MPa), (e) bending structure (at 95 MPa), and (f) tensile direction (at 110 MPa).

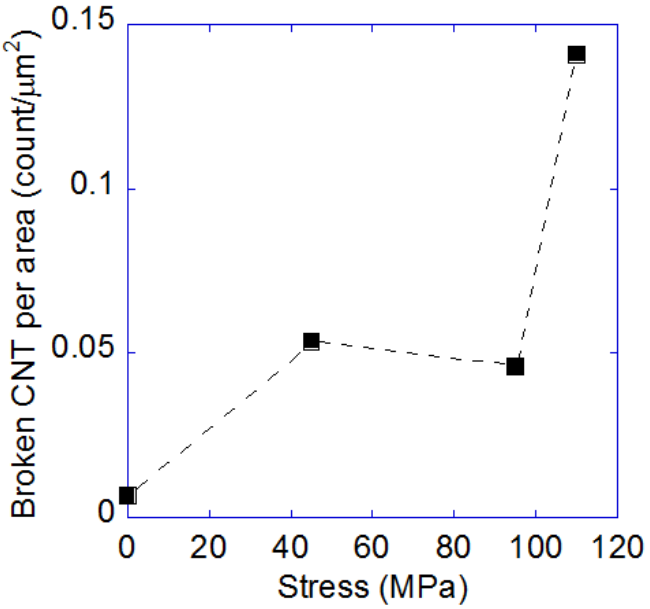


Fig. 6 Relation between stress and broken CNT per area.

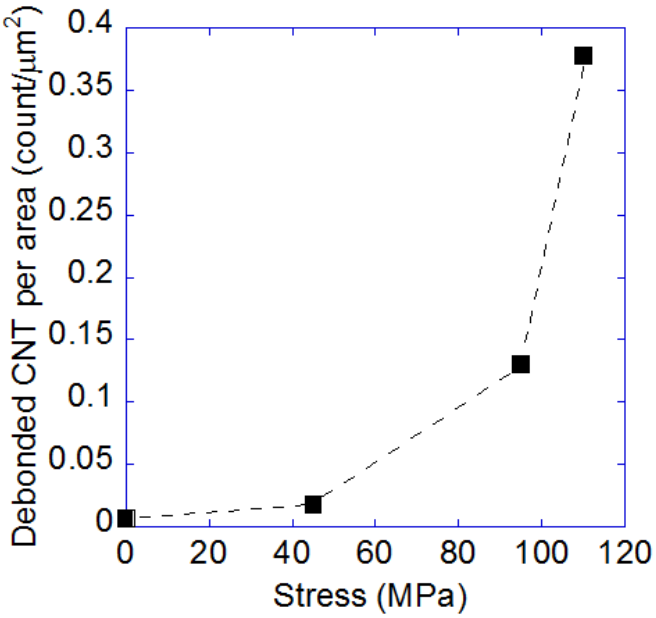


Fig. 7 Relation between stress and debonded CNT per area.

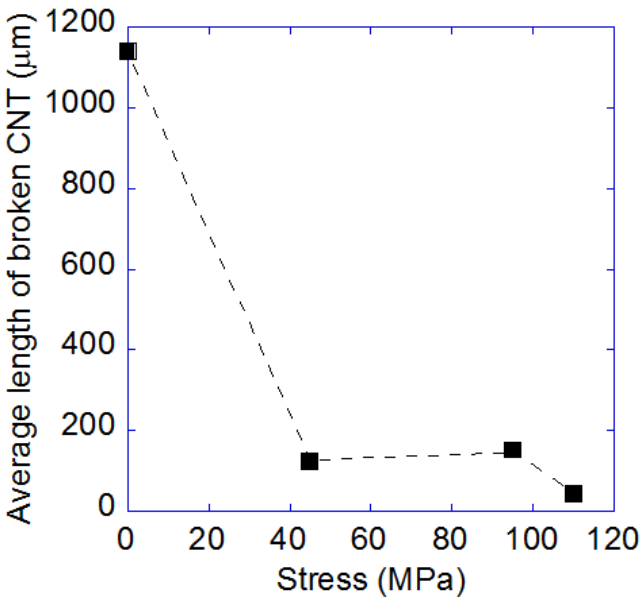


Fig. 8 Relation between stress and average length of broken CNT.

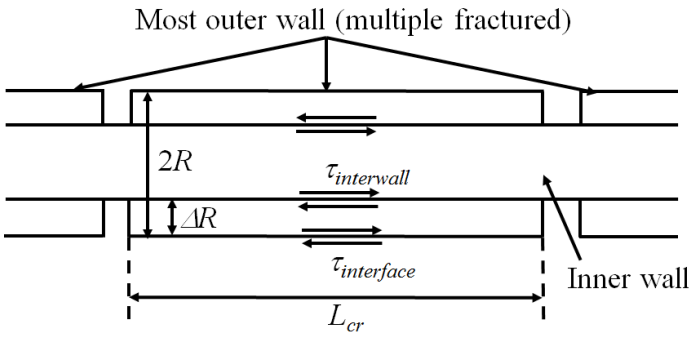


Fig. 9 Load transfer estimation model (for simplicity, inner wall is modeled as fiber).

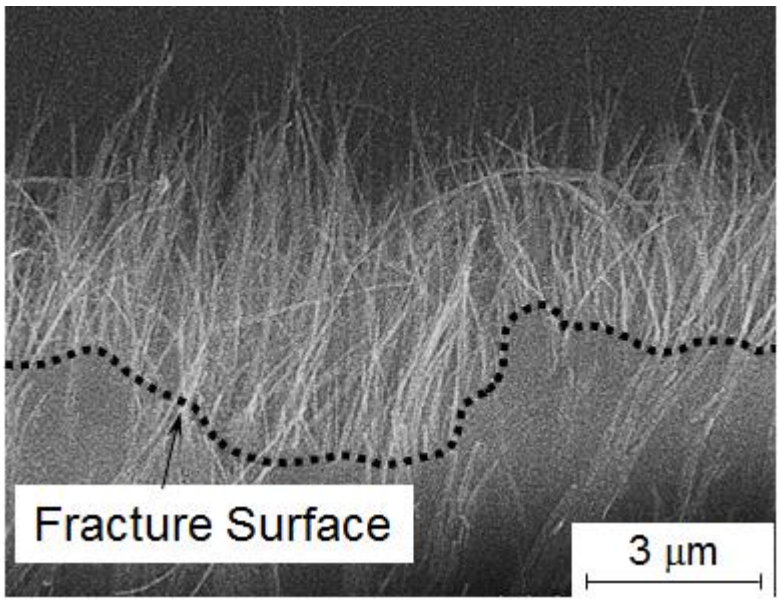


Fig. 10 Fracture surface of the composites. Exposed length of CNTs is 1.0–7.4 μm (average length: 4.1 μm).

Table 1 Fracture analysis results for each stress

| stress (MPa) | CNT count | broken CNT | debonded CNT | observed area ($\mu m^2$) | broken CNT per area ($/\mu m^2$) | debonded CNT per area($/\mu m^2$) |
|---|---|---|---|---|---|---|
| 0 | 912 | 1 | 1 | 149.3 | 0.007 | 0.007 |
| 45 | 654 | 6 | 2 | 112.0 | 0.054 | 0.018 |
| 95 | 846 | 6 | 17 | 130.6 | 0.046 | 0.130 |
| 110 | 1116 | 25 | 67 | 177.3 | 0.141 | 0.378 |

Table 2 Average length of broken CNT for each stress

| Stress (MPa) | CNT count | Total length of CNT (μm) | Average length of broken CNT (μm) (by eq. (1) ) |
|---|---|---|---|
| 0 | 912 | 1139.2 | 1139.2 |
| 45 | 654 | 748.5 | 124.7 |
| 95 | 846 | 914.3 | 152.4 |
| 110 | 1116 | 1115.8 | 44.6 |

Table 3 Results of strength estimation for various methods

| Author | CNT growth | Strength (GPa) | Method |
|---|---|---|---|
| Yu [5] | Arc discharge | 20–63 | Dual AFM cantilevers |
| Demcayk [6] | Arc discharge | 150 | TEM-direct tension |
| Pan [7] | CVD | 1.72 ± 0.64 | Stress–strain puller |
| Peng [8] | CVD | 35–110 | TEM–MEMS testing system |
| This study | CVD | 34.2 | Eq. (2) from internal fracture observation by TEM |
| This study | CVD | 3.2–22.7 (12.7) | Eq. (5) and Eq. (2) from fracture surface observation |
| This study | CVD | 8.9 | Eq. (2) from internal fracture observation by TEM (including interfacial debonding) |
| This study | CVD | 0.8–5.9 (3.3) | Eq. (5) and Eq. (2) from fracture surface observation by SEM (including interfacial debonding) |
| This study | CVD | 1307 | Eq. (2) from internal fracture observation by TEM (Only outermost wall is considered) |
| This study | CVD | 488 | Eq. (5) and Eq. (2) from fracture surface observation (Only outermost wall is considered) |
| This study | CVD | 342 | Eq. (2) from internal fracture observation by TEM (including interfacial debonding, only outermost wall is considered) |
| This study | CVD | 127 | Eq. (5) and Eq. (2) from fracture surface observation by SEM (including interfacial debonding, only outermost wall is considered) |
| This study | CVD | 1.36 | Stress–strain curve and volume fraction of CNT |
| This study | CVD | 1.94 | Eq. (6) from stress–strain curve and Weibull distribution |
| This study | CVD | 52.3 | Stress–strain curve and volume fraction of CNT (only outermost wall is considered) |
| This study | CVD | 74.7 | Eq. (6) from stress–strain curve and Weibull distribution (only outermost wall is considered) |